Effect of Sintering Temperature on the Microstructure Behavior of Gelcasted Porous Ceramics Using Cassava Starch as Pore Template

Suriati Eka Putri[1], Diana Eka Pratiwi[1], Rachmat Triandi Tjahjanto[2], Nita Magfirah Ilyas[1], Dahlang Tahir[3], Abd Rahman[4], and Heryanto Heryanto[3*]

[1]*Department of Chemistry, Faculty of Mathematics and Natural Sciences, Universitas Negeri Makassar, Jl. Daeng Tata, Makassar 90244, Indonesia*

[2]*Department of Chemistry, Faculty of Mathematics and Natural Sciences, Brawijaya University, Jl. Veteran, Malang 65145, Indonesia*

[3]*Department of Physics, Faculty of Mathematics and Natural Sciences, Hasanuddin University, Jl. Perintis Kemerdekaan Km. 20, Makassar 90245, Indonesia*

[4]*Inorganic Chemistry, King Fahd University of Petroleum & Minerals, Academic Belt Road, Dhahran 31261, Saudi Arabia*

* ***Corresponding author:***

email: heryanto@science.unhas.ac.id

Received: November 3, 2022
Accepted: May 4, 2023

DOI: 10.22146/ijc.78875

Abstract: *The gelcasting technique was employed to fabricate porous ceramics utilizing kaolinite clay as the base material with a combination of 20 wt.% cassava starch. The utilization of cassava starch as a pore-template material is a sustainable and eco-friendly approach. The dry mixture compacted pellets underwent calcination for 2 h at three distinct sintering temperatures, namely 900, 1000, and 1100 °C. The present study investigated the impact of sintering temperatures on various ceramic properties, including but not limited to porosity, hardness, crystallinity, lattice strain, and morphology. Furthermore, an increase in sintering temperature led to a reduction in crystallinity of the ceramic material from 81.71 to 78.06%, while the lattice strain increased, as determined by the full width at half maximum peak diffraction calculation. The study determined that the pore size remained microporous (21 Å) across all temperature treatments. Ultimately, a porous ceramic material was fabricated, exhibiting a porosity of 39.44% by volume and a desirable hardness of 94 HB. The optimal sintering temperature for this material was found to be 900 °C. The anticipated application of the porous ceramic, which has taken on a pellet shape, is as a catalyst support for wastewater filtration in the future.*

Keywords: *cassava starch; kaolinite clay; sintering*

■ INTRODUCTION

Customized porosity of materials gives unique qualities and features, which are difficult to be obtained and achieved in conventional materials. Porous materials are being used in many end products and technologies presently. Furthermore, porous materials are also used in many different ways and forms in everyday human life. For example, polymer foams are used for packaging. Lightweight aluminum structures are used in buildings and airplanes while porous ceramics are used to clean water. Porous ceramics provide the opportunity to combine high porosity with crucial properties such as high thermal conductivity, high strength, and chemical stability, which are essential for industrial applications and development. The implementation of the materials includes catalytic support [1-2], removal of heavy metal ions or azo dyes from wastewater [3-4], thermal insulators [5], combustion analyzers [6], and membrane for microfiltration [7]. However, due to pricey raw materials and production techniques, the usage of porous ceramics in more widespread applications is restricted [8]. Therefore, the development of porous

materials made from natural resource materials and the fabrication route using low temperatures are of interest and goal in this study.

Several methods have been employed to fabricate porous ceramics, including the direct consolidation method [9], fused deposition [10], freeze casting [11], gelcasting [12], foam gelcasting [13], and sol-gel [14]. Among these methods, gelcasting is a simple low-cost method because the fabrication process does not require high temperatures and pressures [15]. Gelcasting is one method of shaping process that is entirely developed with basic principles of *in-situ* polymerization of monomers in a ceramic slurry, creating a strong, cross-linked polymer-solvent gel that acts as a pore template [16]. Our previous research produced porous ceramic by the gelcasting method, and the material has good properties (high porosity with high ceramic body strength) as adsorbent for azo dyes [2]. In addition, Han et al. [17] also produced a porous ceramic body with good thermal conductivity for heat insulation applications. As a result, gelcasting will unquestionably become a crucial technique for producing ceramic parts in various shapes.

The most often used gel, acrylamide (AM), is a neurotoxic, and the raw materials employed are synthetic metal oxide powders such alumina, nitride, and zirconia [18-19], which is expensive. As a result, the industry is hesitant to use the gelcasting technology. Therefore, it is necessary to discover alternative natural polymers and raw materials. Several natural polymers, such as chitosan [18], rice flour [20], cassava starch [21], and egg white [22], have been developed as pore templates by several researchers. The raw material that has attracted the attention of researchers is clay [23]. Besides being quite abundant, this natural mineral also has good chemical resistance, good thermal stability, and good mechanical properties.

Liu et al. [24] have successfully used natural clay as a raw material in the gelcasting process to fabricate porous ceramics and reported that porosity could be controlled by adjusting sintering temperatures. In addition, low-cost porous ceramics by gelcasting method using clay have also been successfully carried out with a sintering temperature of 1100–1500 °C, reporting that by adjusting sintering temperatures, pore size distribution and gas permeability can be controlled [25]. However, both of these studies still use AM as a gelling agent. As for the use of cassava starch as a pore template, we have observed previously. The resulting porous ceramics can be used as catalyst support [26]. In addition, Barros Calado et al. [27] using a combination of sunflower oil as a gelling agent and starch consolidation, reported that the manufacturing methods were effective in the production of cellular porous ceramics with low energy, low amounts of gelling agent and low environmental costs. However, the raw material used is synthetic metal oxide powder, i.e., alumina. Based on these perspectives, the challenge to investigate how the sintering temperature affects the microstructure behavior of porous ceramics is necessary for this field. As an improvement, the base material made of clay and cassava starch is applied, which is certainly more environmentally friendly and can be suggested for the industry. To the best of our knowledge, no previous studies have investigated the combination of clay as raw material and cassava starch as a pore template. In addition, quantitative analyses to illustrate the relationship between crystallinity and crystallite size to the porosity response of ceramics are also reported in detail.

■ EXPERIMENTAL SECTION

Materials

Natural clay was taken from South Sulawesi (was slightly ground and sieved to pass 60 mesh, containing 71.12 wt.% SiO_2, 11.98 wt.% Al_2O_3, 5.68 wt.% Fe_2O_3, and less than 0.80 wt.% of TiO_2, CuO, K_2O, ZnO by XRD analysis). The cassava starch (containing 59.97% of starch) and carboxy methyl cellulose (CMC) were used as the dispersant.

Instrumentation

Determination of thermal treatment

Thermal analysis using the thermogravimetric (TG) and differential thermal analysis (DTA) Hitachi STA7300 was used to determine the thermal treatment. On an alumina crucible, 5.947 mg of gelcasted green

body ceramic was weighed. It was isothermally heated at 30 °C for 10 min under airflow (8 L/min) and then heated to 1100 °C in a static air environment. The reference material was alumina, and the heating rate was 30 °C/min.

Mechanical stability

Mechanical stability was measured using Galdabini's Universal Testing Machine (UTM) type PM 100, with a cross-sectional area of 20 × 20 mm.

Chemical stability

Chemical stability is determined by acid and alkali resistance, which is calculated by the weight loss after acid and alkali treatment. The acid solution used is 50% H_2SO_4, while the alkali solution is NaOH is 35% aqueous solution, porous ceramics soaked with chemical reagents for a day.

Procedure

As much as 5 g of natural clay and 0.1 g of CMC were added to distilled water in a ratio of 50:1 (50% vol). Then, the aqueous suspension was added to cassava starch of 9 wt.% [27]. The suspension was moulded, aerated to dry, and heated at 70 °C for 2 h, resulting in gelcasted green body ceramics. After that, the body ceramic was sintered at 900, 1000, and 1100 °C with a heating rate is 50 °C/30 min and thermal treatment based on TGA/DTA results. The fabrication scheme of porous ceramic by gelcasting method in the study as shown in Fig. 1.

Sample characterization

The phase of the specimen was characterized by X-ray diffraction (XRD, Shimadzu 7000) with CuKα radiation (λ = 1.5405 Å). The average crystallite size was determined by the Debye-Scherrer equation. The microstructures of the specimen were observed by scanning electron microscopy (SEM, JEOL-6000PL), which qualitatively indicated a grain size of 60 mesh. The quantitative analysis was also examined with energy dispersive analysis (EDX), and phase quantification was obtained from SEM-EDX maps by processing EDX area maps using Image JED-2300 software.

Mass shrinkage is determined by calculating the ratio of the difference between the mass of the specimen before and after sintering to the mass before sintering. The bulk density and apparent porosity were measured by the Archimedes principle according to the ASTM C373-88. The hardness test (Hardness Brinell/HB) of porous ceramic samples is made using a microhardness tester. Ceramics are smoothed using Ipolising and sandpaper. Ceramics are placed on the stand and then pressed by a steel ball with a diameter of 10 mm and a load of 5 kg in order to determine the magnitude of hardness.

The pore characteristic of the specimen, including surface area, pore volume, and pore distribution, was determined by adsorption N_2 using a surface area analyzer (SAA, type Quantachrome Nova 4200e) with outgas time

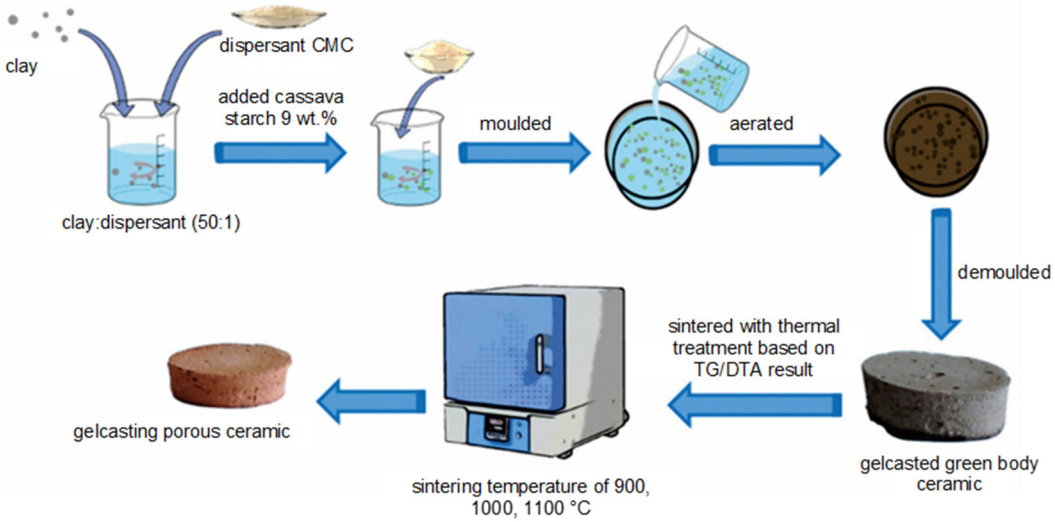

Fig 1. Schematic illustration of fabrication porous ceramic by gel casting method

of 3 h at a temperature of 250 °C. The textural characteristics, such as surface area and pore volume, were determined through the application of the Brunauer-Emmet-Teller (BET) method. The total pore volume was estimated by measuring the amount of adsorbed gas at a relative pressure of $P/P_0 = 0.99$. Additionally, the pore distribution was analyzed using the Barret-Joyner-Halenda (BJH) method.

■ RESULTS AND DISCUSSION

Thermal Cycling

Thermal treatment is an extremely important step in the porous ceramic manufacturing process. In this study, the stages of thermal treatment based on TGA/DTA analysis of gelcasted green body ceramics are shown in Fig. 2. The results showed there are three stages of weight loss during heating. The first stage, noted by the elimination of free and physically adsorbed water from the piece's surface as well as in the starch consolidation, occurs between 25 and 130 °C with a weight loss of 31.66%. This phenomenon agreed with Barros Calado et al. [27]. The second stage corresponds to 23.33% of weight loss at a temperature between 150 and 390 °C possibly due to the thermal decomposition of starch beginning and continuing in the third step with oxidative decomposition. This phenomenon is followed by the exothermic peak at 385 °C on the DTA curve. It is estimated that at this stage, the formation of pores on the green body ceramic has started to occur. The third stage occurs between 400 and 600 °C with a weight loss of 12.80%, possibly due to carbon dioxide released by the degradation of the starch polymer and the release of the hydroxide group from aluminum hydroxide to alumina, respectively [28]. It is also supported by Nie and Lin [29], which reported that the crucial temperature range for burning starch out before ceramic sintering is from 300 to 600 °C.

In addition, the DTA thermogram showed, at 460 °C, an exothermic peak, as shown by the formation of a down peak, indicating the rearrangement of metal oxides to become denser; hence, an exothermic peak develops after 500 °C. Additionally, at temperatures between 600 and 1000 °C associated with the phase transformation from

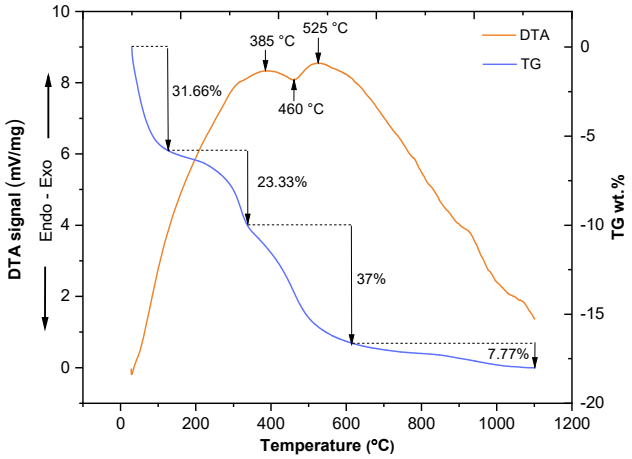

Fig 2. Thermal analysis of gelcasted green body ceramic using TGA/DTA

meta kaolinite to Al-Si spinel [30]. Thus, thermal treatment is carried out by holding temperatures at 100, 400, and 600 °C for 1 h followed by sintering with temperature variations of 900, 1000, and 1100 °C for 2 h.

Mineralogy and Crystallinity

The XRD patterns of the samples sintered at 900, 1000, and 1100 °C are shown in Fig. 3. The crystalline phases are identified as quartz (SiO_2) PDF# 00-046-1045 as a main phase existing in clay [31], mullite ($3SiO_2{\cdot}2Al_2O_3$) PDF# 00-002-0452, and hematite (Fe_2O_3) PDF# 00-002-0919. As the sintering temperature is raised to 1100 °C, the orthoclase ($(Na,K)(Si_3Al)O_8$) PDF# 00-009-0478 reflection intensities increase while the quartz reflection starts to decrease as a result of consumption by the ongoing mineral processes. This agrees with Lu et al. [32] who reported the partial dissolution of quartz in glass melts facilitating the nucleation and crystallization of the anorthite phase. The formation of anorthoclase indicates that the Si sites in the clay are retaining the K released at a temperature over 1000 °C [33]. As a result, the produced porous ceramic's mineralogical phases are considerably influenced by the sintering temperature.

In addition, the sintering temperature also affects the crystallinity, crystallite size, and microstrain of samples, as shown in Fig. 4. Crystallinity increased with increasing temperature to 1000 °C and decreased significantly when the sintering temperature was increased to 1100 °C.

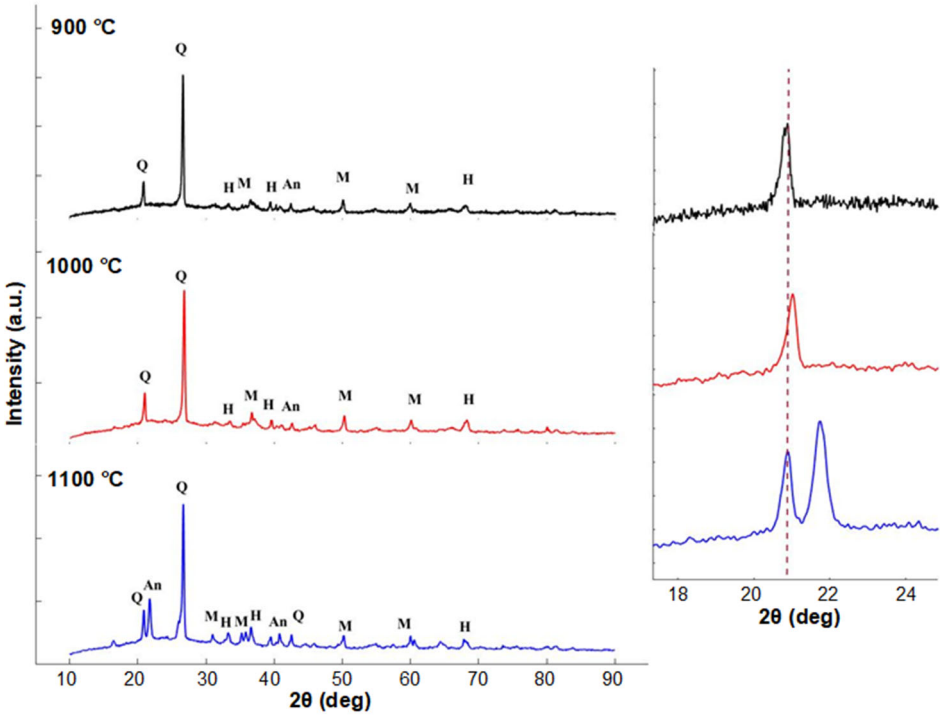

Fig 3. XRD patterns of gelcasted porous ceramics, and the enlarged of spectrum to shows the phase shift as the result of with various sintering temperatures. Q: Quartz, An: Anorthoclase, M: Mullite, H: Hematite

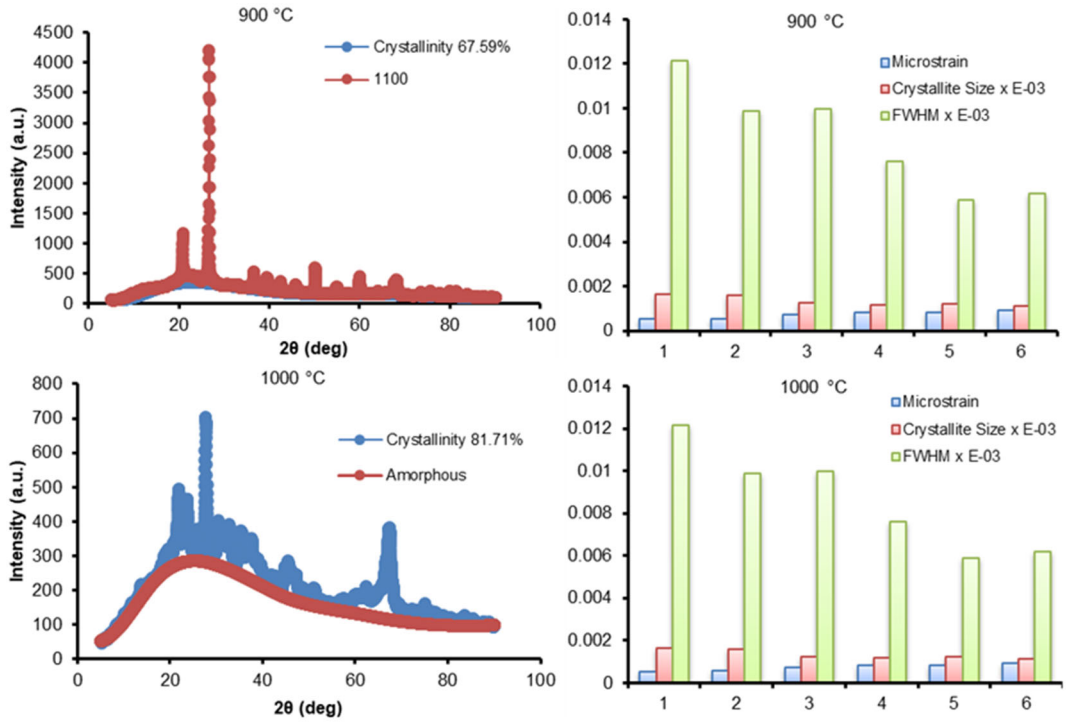

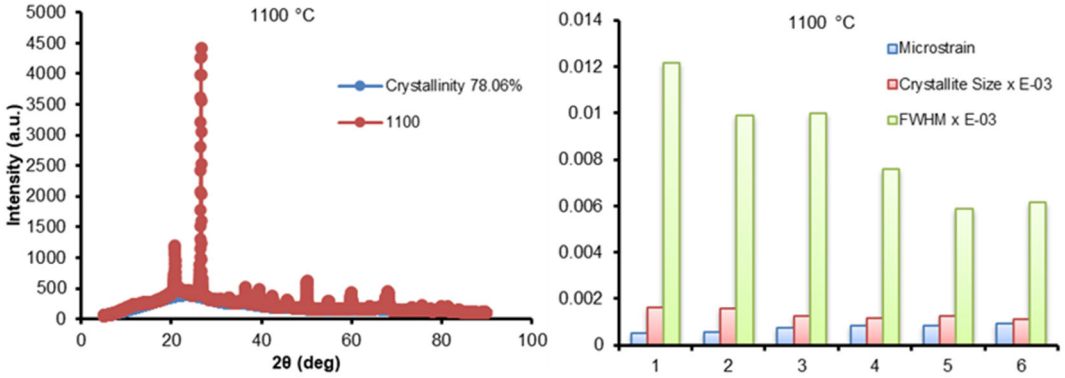

Fig 4. The evaluation of crystallinity, the crystallite size, and microstrain vs full-width half maximum

This is due to the melting of the microstructure typical of the sintering liquid phase and can be attributed to the decrease in mullite intensity (Fig. 3) with increasing sintering temperature. The increase in crystallinity up to 1100 °C was observed with full width at half maxima (FWHM) and did not change with increasing sintering temperature. Sintering temperature up to 1100 °C does not change the crystal phase but only causes an increase in the intensity of the diffraction peak [34].

From the maximum peak FWHM amount, the crystallite size of specimens calculated using the Debye-Scherrer equation as Eq. (1) [35-36],

$$D = \frac{0.9\lambda}{\beta \cos\theta} \quad (1)$$

where λ (1.5406 Å) is the x-ray wavelength radiation of CuKα, β is the full width at FWHM of the diffraction peak, and θ is the Bragg angle. Based on Fig. 4, the crystallite size increased with the increasing sintering temperature of 1000 °C and increased at 1100 °C. It is well known that the higher sintering temperature promotes grain growth, and consequently, crystallite size increases as a function of sintering temperature [37]. The present investigation reveals that the samples' crystallite size exhibited a decreasing trend with an increase in sintering temperature up to 1100 °C. The observed anomalous behavior may be accounted for by positing a significant increase in defect concentration resulting from densification at a temperature of 1000 °C. This phenomenon may be attributed to the relatively low degree of crystallinity exhibited by the specimen at the sintering temperature of 1000 °C, as evidenced by Fig. 4, and the consequent rapid deformation of particles. The utilization of the Williamson-Hall method was employed to verify the structural parameters of the specimens, whereby the strain was determined through the application of Eq. (2).

$$B_{hkl} \cos\theta = \frac{k\alpha}{D} + (4\varepsilon \sin\theta) \quad (2)$$

When using the Williamson-Hall calculation method, it is presumed that the strain is constant throughout crystallographic space and that the material's characteristics are independent of space [38]. Fig. 4 shows the correlation between crystallite size and microstrain; the smaller crystallite size, the microstructure increases. This is corresponded by Venkatesh et al. [39], reported that the decrease in the FWHM of the diffraction peaks with sintering temperature, indicating an improvement in the crystallization process by elimination of defects such as voids or vacancies, crystallite growth, and crystallite coalescence.

Surface Morphology

The SEM images of the samples sintered at 900, 1000, and 1100 °C are shown in Fig. 5. The surface morphology shows heterogeneous microstructures with large pores in the sample sintered at 900 °C. The high porosity is responsible for the thermal degradation of starch. The sample is more microstructurally dense when sintered at 1000 °C, but the porosity is still significant, which can be attributed to a lack of vitreous phase to completely fill all the narrow pores. In contrast, the number of narrow pores decreases at a sintering temperature of 1100 °C, due to the fluxing effects of these

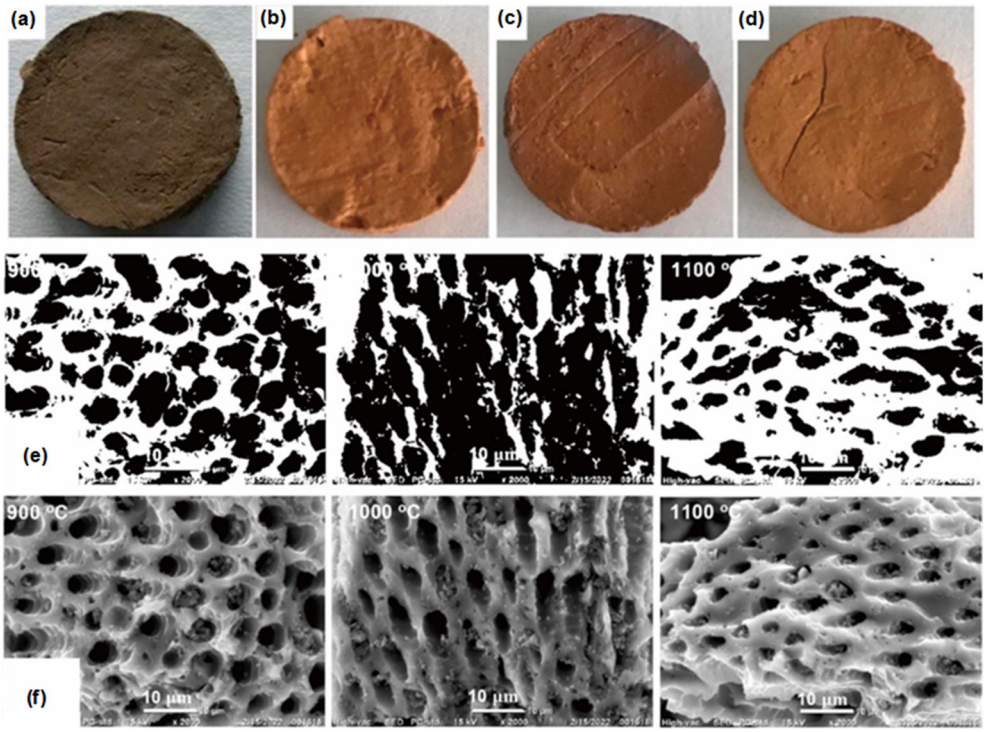

Fig 5. Digital photos of (a) green body porous ceramic, sintered porous ceramic at temperatures (b) 900 °C, (c) 1000 °C, (d) 1100 °C, (e) grayscale of SEM image for more visibility of porosity boundary, (f) SEM images of samples with various sintering temperature with 2000× magnification

oxides. The presence of alkaline-rich phases in the sample speeds up the vitrification process [40]. A vitreous phase may also be induced by the amorphous silica produced during the breakdown of metakaolin [33]. As the temperatures increase, the number of narrow pores is decreased by this phase's binds the particles strong.

Apparent Porosity, Density, and Hardness

The sintering temperatures have a significant effect on the apparent porosity, density, and hardness of gelcasted porous ceramics, as shown in Table 1. Porosity decreases as the sintering temperature increases, which parallels the increase in mass shrinkage and density. It can be explained by body densification, which promotes partial removal of porosity at high temperatures. This result is supported by the results obtained by SEM (Fig. 5), where the formation of the vitreous phase increases with the highest sintering temperature [33]. When the sintering temperature was increased to 1100 °C the porosity decreased, and the mass shrinkage and density increased. This is due to the driving force of densification increased. Thus, when excessive sintering temperature leads to the collapse of the ceramic structure, and therefore, cracks in the ceramic body are observed (Fig. 6). These results imply that there is an upper limit for sintering.

Based on the result of chemical stability, the porosity of ceramic has a significant impact on the chemical stability of specimens. Based on Fig. 5(e) and (f), the increase in porosity will deteriorate the chemical resistance of the specimen. It can be attributed to the increasing porosity of a material, the easier it is for acids and bases to be adsorbed [15], which can be associated with a decrease in the hardness of the specimen. The porous ceramic is least resistant in sulfuric acid solution than in sodium hydroxide solution. Chemical stability results were carried out with two different solvents, such as acid and alkali solutions. The stability results can be written as follows: (1) in acid solution are presented 0.0350 ± 0.002, 0.0027 ± 0.019, and 0.0110 ± 0.006% for 900, 1000, and 1100 °C, respectively; (2) in alkali solution are presented 0.022 ± 0.015, 0.009 ± 0.013, and 0.008 ± 0.008% for 900, 1000, and 1100 °C, respectively. These

Table 1. Effect of sintering temperature on mass shrinkage, apparent porosity, density, and hardness of gelcasted porous ceramics

Sintering temperature (°C)	Mass shrinkage (%)	Apparent porosity (%)	Density (g/cm^3)	Hardness (HB)	Ref.
900	12.93 ± 0.20	39.44 ± 0.30	10.54 ± 0.02	94.00	This study
1000	16.37 ± 0.10	37.88 ± 0.20	18.56 ± 0.02	101.00	This study
1100	20.48 ± 0.20	29.19 ± 0.20	46.88 ± 0.01	108.00	This study
500	18.70	0.00	-	25.27 ± 1.00	
600	18.60	0.20	-	22.74 ± 1.50	[41]
700	9.15	26.80	-	6.87 ± 1.20	
1350	17.42	11.17	-	5.80	
1400	20.79	4.42	-	7.70	[42]
1450	21.73	1.19	-	11.10	
1500	22.66	0.29	-	13.20	
1550	22.33	0.42	-	12.50	
1250	0.48 ± 0.17	50.56 ± 0.30	1.37 ± 0.01	25.95 ± 3.46	[43]
1550	2.38 ± 0.62	48.05 ± 1.45	1.44 ± 0.04	36.00 ± 9.28	[43]
1270	15.30	49.90	0.97	-	[44]
1100	-	50.00	1.05	-	[45]
800	-	50.20	1.26	-	[46]

Note for (-) is not reported

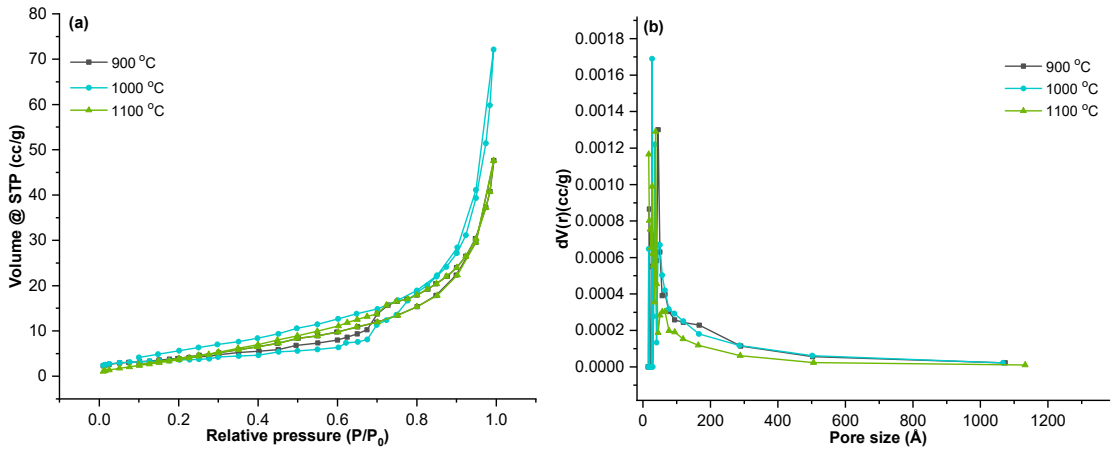

Fig 6. (a) Isotherm of adsorption-desorption curves and (b) pore size distribution of samples

results are associated with the presence of iron compounds in the ceramic body according to the results of the XRD analysis in Fig. 3, which then react with acids to form water-soluble iron sulfate compounds and exchange alkaline ions contained in the ceramic body with hydrogen ions from the acid. The results of the XRD analysis also indicated the presence of silica in the form of quartz. The low acid resistance is also caused by the hydrolysis of the Si–O bond, which is known as the breakdown of the silica framework.

The hardness of samples increases when the sintering temperature increases and is inversely proportional to porosity. The increase of hardness properties at the sintering temperature of 1100 °C was due to the progressive formation of anorthoclase (a vitreous phase that fills the narrow pores) and mullite (strong crystalline phase) (as shown in Fig. 3), which increases the mechanical strength [47]. However, in order to obtain porous ceramic with high porosity (39.44%) and sufficient hardness property (94.00 HB),

Table 2. Pore characteristics of samples

Sintering temperatures (°C)	S_{BET} (m^2/g)	Vt (cm^3/g)	Average pore diameter (Å)
900	16.58	0.14	21.26
1000	17.83	0.09	21.19
1100	16.61	0.13	21.41

the optimal temperature suitable for sintering is 900 °C. The resulting hardness is almost the same as the results of our previous study using acrylamide polymer as a pore template [48]. For the result of mechanical stability, the effect of sintering temperature shows linear results on compression strength. Specimen dimensions were used as a benchmark in determining sample mechanics, where the 1100, 1000, and 900 °C have pressure results with 10.90, 10.27, and 9.56 MPa, respectively. This difference in pressure resistance can be influenced by changes in microstructure and d-spacing properties at the unit crystal scale [49-51].

Pore Characteristics

Pore characteristics consist of specific surface area (S_{BET}), volume total (V_t), and average pore diameter are shown in Fig. 6 and the corresponding in Table 2. There are no obvious hysteresis loops, as can be seen in the N_2 adsorption-desorption isotherms curves of the samples (Fig. 5(a-d). According to the Brunauer-Deming-Deming-Teller classification, the adsorption isotherms for all samples are close to type III, indicating the interaction of the adsorbate with the adsorbed layer is greater than the interaction with the adsorbent surface [52].

Based on Table 2, the pore characteristics of gelcasted porous ceramic are not affected by sintering temperatures. The specific surface area in this study is higher when compared to our previous study, which used polyacrylamide as the pore template [53]. The specific area observed by Salomão and Brandi [54] which used chitosan as a pore template of 7 m^2/g, is lower than in this study. The average pore size of all samples was microporous, indicating the material suitable as a support catalyst and wastewater filter [55]. The specific surface area increases at the sintering temperature of 900 to 1000 °C, and decreases at 1100 °C. This is related to the formation of the molten phase at temperatures above 1000 °C, which promotes sintering of the liquid phase [8]. However, this contradicts the apparent porosity of the sample (Table 1), which shows a decrease in porosity with increasing sintering temperature. This anomalous behavior is thought to be related to the defects produced during densification which are associated with sample crystallinity and rapid particle deformation [32].

■ CONCLUSION

Porous ceramics were formed by the gelcasting method using clay and cassava starch. Pore formation was largely caused by the thermal degradation of starch so a thermal study was carried out using TGA/DTA to determine thermal cycling. The crystalline phase is identified as quartz, mullite, and hematite for the samples sintered at 900, 1000, and 1100 °C. Based on the XRD results, the crystallinity of the ceramic decreased while the lattice strain increased when the sintering temperature increased. Then, the porosity of the ceramic decreased with increasing sintering temperatures. The hardness properties were significantly improved as the sintering temperatures were increased from 900 to 1100 °C. The pore characteristics are not affected by sintering temperatures, and the average pore size for all samples was microporous. The findings imply that the sintering temperature can be used to continually regulate the microstructure properties of porous ceramics based on clay.

■ ACKNOWLEDGMENTS

This work was supported by DRTPM Ministry of Education, Culture, Research, and Technology Republic of Indonesia in the scheme of *Penelitian Dasar Unggulan Perguruan Tinggi* (PDUPT) contract number 109/UN36.11/LP2M/2021 and *Lembaga Penelitian dan Pengabdian Masyarakat* (LP2M) Universitas Negeri Makassar that has held writing workshops of scientific

articles in reputable international journals as a forum for the creation of this research article.

■ AUTHOR CONTRIBUTIONS

Suriati Eka Putri conducted the experiment and wrote the manuscript, Diana Eka Pratiwi revised the manuscript, Rachmat Triandi Tjahjanto and Dahlang Tahir did proofreading the manuscript, Nita Magfirah Ilyas conducted the TGA/DTA analysis, Abd Rahman conducted the BET and BJH calculations, and Heryanto conducted the XRD analysis and finalization. All authors agreed to the final version of this manuscript.

■ REFERENCES

[1] Guo, W., Hu, T., Qin, H., Gao, P., and Xiao, H., 2021, Preparation and *in situ* reduction of Ni/SiC_xOy catalysts supported on porous SiC ceramic for ethanol steam reforming, *Ceram. Int.*, 47 (10, Part A), 13738–13744.

[2] Putri, S.E., Pratiwi, D.E., Tjahjanto, R.T., Hasri, H., Andi, I., Rahman, A., Ramadani, A.I.W.S., Ramadhani, A.N., Subaer, S., and Fudholi, A., 2022, The renewable of low toxicity gelcasting porous ceramic as Fe_2O_3 catalyst support on phenol photodegradation, *Int. J. Des. Nat. Ecodyn.*, 17 (4), 503–511.

[3] Putri, S.E., Pratiwi, D.E., Triandi, R., Mardiana, D., and Side, S., 2018, Performance test of gelcasted porous ceramic as adsorbent of azo dyes, *J. Phys.: Conf. Ser.*, 1028, 012039.

[4] Kim, I.J., Park, J.G., Han, Y.H., Kim, S.Y., and Shackelford, J.F., 2019, Wet foam stability from colloidal suspension to porous ceramics: A review, *J. Korean Ceram. Soc.*, 56 (3), 211–232.

[5] Chen, Y., Wang, N., Ola, O., Xia, Y., and Zhu, Y., 2021, Porous ceramics: Light in weight but heavy in energy and environment technologies, *Mater. Sci. Eng.: R: Rep.*, 143, 100589.

[6] Ismail, A.K., Abdullah, M.Z., Zubair, M., Jamaludin, A.R., and Ahmad, Z.A., 2016, Effect of ceramic coating in combustion and cogeneration performance of Al_2O_3 porous medium, *J. Energy Inst.*, 89 (1), 81–93.

[7] Fontão, N.C., Ferrari, L.N., Sapatieri, J.C., Rezwan, K., and Wilhelm, M., 2022, Influence of the pyrolysis temperature and TiO_2-incorporation on the properties of SiOC/SiC composites for efficient wastewater treatment applications, *Membranes*, 12 (2), 175.

[8] Akhtar, F., Rehman, Y., and Bergström, L., 2010, A study of the sintering of diatomaceous earth to produce porous ceramic monoliths with bimodal porosity and high strength, *Powder Technol.*, 201 (3), 253–257.

[9] Nepomuceno, M.C.S., Bernardo, L.F.A., Pereira-de-Oliveira, L.A., and Timóteo, R.O., 2021, Cement-based grouts for masonry consolidation with high content of limestone filler, metakaolin, glass powder and ceramic waste, *Constr. Build. Mater.*, 306, 124947.

[10] Liu, K., Zhou, C., Chen, F., Sun, H., and Zhang, K., 2020, Fabrication of complicated ceramic parts by gelcasting based on additive manufactured acetone-soluble plastic mold, *Ceram. Int.*, 46 (16, Part A), 25220–25229.

[11] de Morais Santos, L.N.R., de Melo Cartaxo, J., Silva, J.R.S., Rodrigues, A.M., de Andrade Dantas, E.L., de Sousa, F.B., de Araújo Neves, G., and Menezes, R.R., 2021, High porous ceramics with isometric pores by a novel saponification/gelation/freeze-casting combined route, *J. Eur. Ceram. Soc.*, 41 (14), 7111–7118.

[12] Shahbazi, H., and Tataei, M., 2019, A novel technique of gel-casting for producing dense ceramics of spinel ($MgAl_2O_4$), *Ceram. Int.*, 45 (7, Part A), 8727–8733.

[13] Hooshmand, S., Nordin, J., and Akhtar, F., 2019, Porous alumina ceramics by gel casting: Effect of type of sacrificial template on the properties, *Int. J. Ceram. Eng. Sci.*, 1 (2), 77–84.

[14] Jesus, M.A.M.L., Ferreira, A.M., Lima, L.F.S., Batista, G.F., Mambrini, R.V., and Mohallem, N.D.S., 2021, Micro-mesoporous TiO_2/SiO_2 nanocomposites: Sol-gel synthesis, characterization, and enhanced photodegradation of quinoline, *Ceram. Int.*, 47 (17), 23844–23850.

[15] Han, L., Li, F., Zhang, H., Dong, L., Pei, Y., Zhu, Q., Wu, W., Jia, Q., and Zhang, S., 2019, Low-temperature preparation of porous diatomite ceramics via direct-gelcasting using melamine and boric acid as cross-linker and sintering agent, *Ceram. Int.*, 45 (18, Part A), 24469–24473.

[16] Jana, D.C., Sundararajan, G., and Chattopadhyay, K., 2017, Effect of monomers content in enhancing solid-state densification of silicon carbide ceramics by aqueous gelcasting and pressureless sintering, *Ceram. Int.*, 43 (6), 4852–4857.

[17] Han, L., Li, F., Huang, L., Zhang, H., Pei, Y., Dong, L., Zhang, J., and Zhang, S., 2018, Preparation of Si_3N_4 porous ceramics via foam-gelcasting and microwave-nitridation method, *Ceram. Int.*, 44 (15), 17675–17680.

[18] Bengisu, M., and Yilmaz, E., 2002, Gelcasting of alumina and zirconia using chitosan gels, *Ceram. Int.*, 28 (4), 431–438.

[19] Kandi, K.K., Thallapalli, N., Kumar, M.S., and Raod, C.S.P., 2019, Fabrication and parametric optimization of SiO_2-BN gelcast ceramic composites using response surface methodology, *Mater. Today: Proc.*, 18, 2298–2307.

[20] Wan, W., Huang, C., Yang, J., and Qiu, T., 2014, Study on gelcasting of fused silica glass using glutinous rice flour as binder, *Int. J. Appl. Glass Sci.*, 5 (4), 401–409.

[21] Luchese, C.L., Spada, J.C., and Tessaro, I.C., 2017, Starch content affects physicochemical properties of corn and cassava starch-based films, *Ind. Crops Prod.*, 109, 619–626.

[22] He, X., Su, B., Zhou, X., Yang, J., Zhao, B., Wang, X., Yang, G., Tang, Z., and Qiu, H., 2011, Gelcasting of alumina ceramics using an egg white protein binder system, *Ceram.-Silik.*, 55 (1), 1–7.

[23] Mohammed, M.N., Yusoh, K., and Haji Shariffuddin, J.H., 2020, Thermal and structure analysis based on exfoliation of clay in thermosensitive polymer by *in-situ* polymerization, *Indones. J. Chem.*, 20 (1), 88–95.

[24] Liu, Y.F., Liu, X.Q., Wei, H., and Meng, G.Y., 2001, Porous mullite ceramics from national clay produced by gelcasting, *Ceram. Int.*, 27 (1), 1–7.

[25] Liu, Y.F., Liu, X.Q., Li, G., and Meng, G.Y., 2001, Low cost porous mullite-corundum ceramics by gelcasting, *J. Mater. Sci.*, 36 (15), 3687–3692.

[26] Putri, S.E., Pratiwi, D.E., Tjahjanto, R.T., and Rahman, A., 2022, The effect of binder concentration on the ability of gelcasting porous ceramics as TiO_2 support catalyst, *Indones. J. Fundam. Sci.*, 8 (1), 51–60.

[27] Barros Calado, C.M., Iturri, M.S., Colonetti, V.C., Constantino de Souza, V., Fernandes, C.P., Hotza, D., and Novy Quadri, M.G., 2021, Green production of cellular ceramics by emulsification of sunflower oil followed by gelcasting and starch consolidation, *J. Cleaner Prod.*, 282, 124468.

[28] Offner, A., Bach, A., and Sauvant, D., 2003, Quantitative review of *in situ* starch degradation in the rumen, *Anim. Feed Sci. Technol.*, 106 (1-4), 81–93.

[29] Nie, Z., and Lin, Y., 2015, Fabrication of porous alumina ceramics with corn starch in an easy and low-cost way, *Ceram.-Silik.*, 50 (4), 348–352.

[30] Low, I.M., and McPherson, I.M., 1988, The structure and composition of Al-Si spinel, *J. Mater. Sci. Lett.*, 7 (11), 1196–1198.

[31] Kagonbé, B.P., Tsozué, D., Nzeukou, A.N., and Ngos, S., 2021, Mineralogical, physico-chemical and ceramic properties of clay materials from Sekandé and Gashiga (North, Cameroon) and their suitability in earthenware production, *Heliyon*, 7 (7), e07608.

[32] Lu, J., Li, Y., Zou, C., Liu, Z., and Wang, C., 2018, Effect of sintering additives on the densification, crystallization and flexural strength of sintered glass-ceramics from waste granite powder, *Mater. Chem. Phys.*, 216, 1–7.

[33] Mouiya, M., Bouazizi, A., Abourriche, A., Benhammou, A., El Hafiane, Y., Ouammou, M., Abouliatim, Y., Younssi, S.A., Smith, A., and Hannache, H., 2019, Fabrication and characterization of a ceramic membrane from clay and banana peel powder: Application to industrial wastewater treatment, *Mater. Chem. Phys.*, 227, 291–301.

[34] Almasri, K.A., Sidek, H.A.A., Matori, K.A., and Mohd Zaid, M.H., 2017, Effect of sintering temperature on physical, structural and optical properties of wollastonite based glass-ceramic derived from waste soda lime silica glasses, *Results Phys.*, 7, 2242–2247.

[35] Jangong, O.S., Heryanto, H., Rahmat, R., Mutmainna, I., Gareso, P.L., and Tahir, D., 2021, Effect of sugar palm fiber (SPF) to the structural and optical properties of bioplastics (SPF/starch/chitosan/polypropylene) in supporting mechanical properties and degradation performance, *J. Polym. Environ.*, 29 (6), 1694–1705.

[36] Suryani, S., Heryanto, H., Rusdaeni, R., Fahri, A.N., and Tahir, D., 2020, Quantitative analysis of diffraction and infra-red spectra of composite cement/$BaSO_4$/Fe_3O_4 for determining correlation between attenuation coefficient, structural and optical properties, *Ceram. Int.*, 46 (11, Part B), 18601–18607.

[37] Singh, L.K., Bhadauria, A., Jana, S., and Laha, T., 2018, Effect of sintering temperature and heating rate on crystallite size, densification behaviour and mechanical properties of Al-MWCNT nanocomposite consolidated via spark plasma sintering, *Acta Metall. Sin. (Engl. Lett.)*, 31 (10), 1019–1030.

[38] Reddy, M.P., Shakoor, R.A., Mohamed, A.M.A., Gupta, M., and Huang, Q., 2016, Effect of sintering temperature on the structural and magnetic properties of $MgFe_2O_4$ ceramics prepared by spark plasma sintering, *Ceram. Int.*, 42 (3), 4221–4227.

[39] Venkatesh, D., Siva Ram Prasad, M., Rajesh Babu, B., Ramesh, K.V., and Trinath, K., 2015, Effect of sintering temperature on the micro strain and magnetic properties of Ni-Zn nanoferrites, *J. Magn.*, 20 (3), 229–240.

[40] Mouiya, M., Bouazizi, A., Abourriche, A., El Khessaimi, Y., Benhammou, A., El hafiane, Y., Taha, Y., Oumam, M., Abouliatim, Y., Smith, A., and Hannache, H., 2019, Effect of sintering temperature on the microstructure and mechanical behavior of porous ceramics made from clay and banana peel powder, *Results Mater.*, 4, 100028.

[41] Feng, D., Ren, Q., Ru, H., Wang, W., Jiang, Y., Ren, S., and Zhang, C., 2019, Effect of oxygen content on the sintering behaviour and mechanical properties of SiC ceramics, *Ceram. Int.*, 45 (18, Part A), 23984–23992.

[42] Liu, P., Li, Z., Xiao, P., Luo, H., and Jiang, T., 2018, Microstructure and mechanical properties of *in-situ* grown mullite toughened 3Y-TZP zirconia ceramics fabricated by gelcasting, *Ceram. Int.*, 44 (2), 1394–1403.

[43] Mohamed Ariff, A.H., Mohamad Najib, M.A., Mohd Tahir, S., As'Arry, A., and Mazlan, N., 2021, Effect of sintering temperature on the properties of porous Al_2O_3-10 wt% RHA/10 wt% Al composite, *Adv. Mater. Process. Technol.*, 7 (3), 417–428.

[44] Lin, K.L., Chang, J.C., Shie, J.L., Chen, H.J., and Ma, C.M., 2012, Characteristics of porous ceramics produced from waste diatomite and water purification sludge, *Environ. Eng. Sci.*, 29 (6), 436–446.

[45] Bahrami, A., Simon, U., Soltani, N., Zavareh, S., Schmidt, J., Pech-Canul, M.I., and Gurlo, A., 2017, Eco-fabrication of hierarchical porous silica monoliths by ice-templating of rice husk ash, *Green Chem.*, 19 (1), 188–195.

[46] Hao, L., Gao, W., Yan, S., Niu, M., Liu, G., and Hao, H., 2019, Preparation and characterization of porous ceramics with low-grade diatomite and oyster shell, *Mater. Chem. Phys.*, 235, 121741.

[47] Aksel, C., 2003, The effect of mullite on the mechanical properties and thermal shock behaviour of alumina–mullite refractory materials, *Ceram. Int.*, 29 (2), 183–188.

[48] Putri, S.E., and Pratiwi, D.E., 2016, The Effect of Mole Ratio of Acrylamide (AM) Monomer and Methylene-bis-acrylamide (MBAM) Crosslinker Toward the Hardmess of Gelcasting Porous Ceramics, *Proceeding of ICMSTEA 2016: International Conference on Mathematics, Science, Technology, Education and their Applications*,

Makassar, Indonesia, 3rd–4th October 2016, 412–415.
[49] Amir, N., Tahir, D., and Heryanto, H., 2023, Synthesis, structural and optical characteristics of activated carbon photocatalysts to adsorb pesticide waste, *J. Mater. Sci.: Mater. Electron.*, 34 (5), 445–458.
[50] Ilyas, S., Heryanto, H., and Tahir, D., 2021, Correlation between structural and optical properties of CuO/carbon nanoparticle in supports the photocatalytic performance and attenuate the electromagnetic wave, *J. Environ. Chem. Eng.*, 9 (1), 104670.
[51] Heryanto, H., and Tahir, D., 2021, The correlations between structural and optical properties of magnetite nanoparticles synthesised from natural iron sand, *Ceram. Int.*, 47 (12), 16820–16827.
[52] Brunauer, S., Deming, L.S., Deming, W.E., and Teller, E., 1940, On a theory of the van der Waals adsorption of gases, *J. Am. Chem. Soc.*, 62 (7), 1723–1732.
[53] Putri, S.E., Pratiwi, D.E., Tjahjanto, R.T., Mardiana, D., and Subaer, S., 2018, On the effect of acrylamide and methylenebicacrylamid ratio on gelcasted ceramic pore character, *J. Chem. Technol. Metall.*, 53 (5), 841–844.
[54] Salomão, R., and Brandi, J., 2013, Macrostructures with hierarchical porosity produced from alumina-aluminum hydroxide-chitosan wet-spun fibers, *Ceram. Int.*, 39 (7), 8227–8235.
[55] Wang, W., Wang, M., Feng, X., Zhao, W., Luan, C., and Ma, J., 2018, Effects of deposition temperature on the structural and optical properties of single crystalline rutile TiO_2 films, *Mater. Chem. Phys.*, 211, 172–176.